

# Connectivity-Based Subdivisions of the Human Right “Temporoparietal Junction Area”: Evidence for Different Areas Participating in Different Cortical Networks

Rogier B. Mars<sup>1,2</sup>, Jérôme Sallet<sup>1</sup>, Urs Schüffegen<sup>1</sup>, Saad Jbabdi<sup>2</sup>, Ivan Toni<sup>3</sup> and Matthew F. S. Rushworth<sup>1,2</sup>

<sup>1</sup>Department of Experimental Psychology, University of Oxford, Oxford, OX1 3UD, UK, <sup>2</sup>Centre for Functional Magnetic Resonance Imaging of the Brain, University of Oxford, Oxford, OX3 9DU, UK and <sup>3</sup>Centre for Cognitive Neuroimaging, Donders Institute for Brain, Cognition, and Behaviour, Radboud University Nijmegen, 6500 HB Nijmegen, The Netherlands

Address correspondence to Rogier B. Mars, Department of Experimental Psychology, University of Oxford, Tinbergen Building, 9 South Parks Road, Oxford, OX1 3UD, UK. Email: rogiar.mars@psy.ox.ac.uk.

**Controversy surrounds the role of the temporoparietal junction (TPJ) area of the human brain. Although TPJ has been implicated both in reorienting of attention and social cognition, it is still unclear whether these functions have the same neural basis. Indeed, whether TPJ is a precisely identifiable cortical region or a cluster of subregions with separate functions is still a matter of debate. Here, we examined the structural and functional connectivity of TPJ, testing whether TPJ is a unitary area with a heterogeneous functional connectivity profile or a conglomerate of regions with distinctive connectivity. Diffusion-weighted imaging tractography-based parcellation identified 3 separate regions in TPJ. Resting-state functional connectivity was then used to establish which cortical networks each of these subregions participates in. A dorsal cluster in the middle part of the inferior parietal lobule showed resting-state functional connectivity with, among other areas, lateral anterior prefrontal cortex. Ventrally, an anterior TPJ cluster interacted with ventral prefrontal cortex and anterior insula, while a posterior TPJ cluster interacted with posterior cingulate, temporal pole, and anterior medial prefrontal cortex. These results indicate that TPJ can be subdivided into subregions on the basis of its structural and functional connectivity.**

**Keywords:** attention, default mode, diffusion-weighted imaging, parietal, reorienting, resting state, social cognition, temporal

## Introduction

“Temporoparietal junction” (TPJ) area is a widely used but approximate term that usually refers to the cortical expanse at the intersection of the posterior end of the superior temporal sulcus (STS), the inferior parietal lobule (IPL), and the lateral occipital cortex in the human brain. TPJ, particularly in the right hemisphere, has been implicated in a number of higher order cognitive functions, related to attentional selection on the one hand (Corbetta and Shulman 2002; Himmelbach et al. 2006) and social cognition on the other hand (Saxe and Kanwisher 2003). However, the precise role of this region, and indeed, whether it is a single region performing an overarching function, perhaps in conjunction with different areas depending on the task at hand or a number of spatially separate subregions involved in separate functions, remains a topic of debate. This debate is complicated by a lack of clarity concerning the location and boundaries of TPJ and uncertainty about its correspondence with areas in nonhuman primates.

According to one influential account of attention, a dorsal attentional network, consisting of the superior parietal lobule and dorsal frontal cortex, is concerned with directing attention

based on current goals and preexisting top-down information, while a ventral attentional network, consisting of TPJ and the ventral prefrontal cortex (vPFC) and anterior insula (AI), is concerned with reorienting of attention in response to behaviorally relevant events from the environment (Corbetta and Shulman 2002). In this framework, the TPJ acts as a “circuit breaker” interrupting ongoing activity in the dorsal attentional network, which in turn shifts attention to the novel information of interest (Astafiev et al. 2006). Consistent with a role in processing of behaviorally relevant events, TPJ has been suggested to be a source of the P300 (Knight et al. 1989; Yamaguchi and Knight 1991), a component of the event-related brain potential associated with the processing of surprising and relevant events (Nieuwenhuis et al. 2005; Mars et al. 2008). Furthermore, interference with TPJ function can lead to attentional deficits such as hemiextinction (Meister et al. 2006). It has been suggested that damage to TPJ is a primary cause of spatial neglect, although this has also been localized to the nearby angular gyrus (Mort et al. 2003).

Investigations of social cognition are also often associated with activation of the same, or closely adjacent, part of cortex. In this context, the function most commonly associated with TPJ is the attribution of mental states to others, such as in theory of mind (ToM) paradigms. These types of tasks can involve participants reading or thinking about stories involving complex mental states (Fletcher et al. 1995; Saxe and Kanwisher 2003; Den Ouden et al. 2005; Frith CD and Frith U 2006) or attempting to make inferences about another person’s intentions (Behrens et al. 2008; Hampton et al. 2008). The common feature of the tasks activating TPJ seems to be that the participant is thinking about, or making predictions about, another person’s mental state, rather than for instance making predictions about other events in the environment or thinking about the physical characteristics of a person (Saxe and Wexler 2005). Indeed, it has been argued that this is the unique defining characteristic of TPJ activity in social tasks (Saxe 2006).

A few studies have compared the relative contribution of the TPJ in attentional selection and in social cognition, in order to test whether they are reflections of the same underlying function. In a meta-analysis of neuroimaging studies, Decety and Lamm (2007) reported that the center of gravity of activations related to ToM is located 14 mm more posterior than the center of gravity of activations related to attentional selection, although there was strong overlap in the location of peak activations in the different studies. These authors therefore suggested a domain general role for the TPJ. Spatial overlap between activations evoked in the TPJ by attentional selection and social-cognitive task involving attribution of

beliefs (ToM) has also been found within a single group of participants (Mitchell 2008). However, the opposite result has also been obtained (Scholz et al. 2009). These studies, however, did not test whether TPJ displays different profiles of functional connectivity during ToM and attentional tasks, as suggested by recent results. For instance, Fox et al. (2006) used resting-state functional connectivity to distinguish between the dorsal and ventral attentional networks. They reported spontaneous correlations between activity in the TPJ and vPFC. In contrast, a recent study investigating functional interactions during a social emotion task reported increased functional connectivity between TPJ and the anterior medial prefrontal cortex (amPFC) (Burnett and Blakemore 2009). Furthermore, social tasks often show coactivation of TPJ and posterior cingulate cortex, a brain region that is not commonly reported in attention tasks (Corbetta et al. 2008).

The debate on whether TPJ consists of one or more subregions may be informed by looking at the connectivity of this area. A brain region's connectivity determines the information it receives and the influence it can exert on other brain areas. As such, the connectivity of a brain region is a strong determinant of its function. Moreover, it has been shown that brain areas defined on the basis of other structural measures, such as cytoarchitecture, display unique patterns of connectivity (Passingham et al. 2002). Measures of connectivity have therefore been used recently to determine the presence of subdivisions in, for example, the premotor and parietal cortex, and these differences have been used to constrain and guide interpretations of their functions (Johansen-Berg et al. 2004; Tomassini et al. 2007; Mars et al. 2011).

In the present study, rather than looking at the loci of activation during different cognitive tasks (Decety and Lamm 2007), we investigate the possibility that the functional heterogeneity of TPJ arises from adjacent but distinct structural subregions that can be distinguished on the basis of their connectivity. These connections can be estimated using a combination of structural and functional connectivity measures. First, we use diffusion-weighted magnetic resonance imaging (DW-MRI) tractography-based parcellation (Johansen-Berg et al. 2004; Anwander et al. 2007; Tomassini et al. 2007; Beckmann et al. 2009) to divide the TPJ into distinct subregions, on the basis of differences in estimated structural connections to the rest of the brain. Then, we use resting-state functional connectivity to investigate with which parts of the brain each of the TPJ subregions interact and thus to determine which larger cortical networks they are part of. We hypothesize that different subregions of TPJ can be distinguished based on differential connectivity with the ventral attentional network, including vPFC and AI, and brain areas associated with social processing such as amPFC.

## Materials and Methods

### Analysis 1: Diffusion-Weighted Imaging Tractography-Based Parcellation

#### Data Acquisition

Diffusion-weighted images were acquired in 8 healthy participants (4 female; age range 20–36, mean age  $\pm$  standard deviation [SD]  $26.9 \pm 6.0$ ) on a 1.5-T Siemens (Erlangen, Germany) Sonata MR scanner, with maximum gradient strength of  $40 \text{ mT} \times \text{m}^{-1}$ . This number of participants has recently been shown to be sufficient to obtain reliable parcellation results (Klein et al. 2007). All participants gave informed written

consent in accordance with ethical approval from the local ethics committee. Participants lay supine in the scanner, and cushions were used to reduce head motion. Diffusion-weighted data were acquired using echo planar imaging (72-  $\times$  2-mm thick axial slices, matrix size  $128 \times 104$ , field of view  $256 \times 208 \text{ mm}^2$ , giving a voxel size of  $2 \times 2 \times 2 \text{ mm}$ ). Diffusion weighting was isotropically distributed along 60 directions using a  $B$  value of  $1000 \text{ s} \times \text{mm}^{-2}$ . For each set of diffusion-weighted data, 5 volumes with no diffusion weighting were acquired throughout the acquisition. Three sets of diffusion-weighted data were acquired for subsequent averaging to improve the signal-to-noise ratio. The total scan time for the diffusion-weighted imaging protocol was 45 min. A structural scan was acquired for each participant in the same session, using a  $T_1$ -weighted 3D FLASH sequence (time repetition [TR] = 12 ms, time echo [TE] = 5.65 ms, flip angle =  $19^\circ$ , with elliptical sampling of  $k$  space, voxel size  $1 \times 1 \times 1 \text{ mm}$ ).

#### TPJ Region of Interest

A region of interest (ROI) was drawn on the right hemisphere of a structural brain in Montreal Neurological Institute (MNI) standard space (Fig. 1). This study concentrated on the TPJ in the right hemisphere, since it is this area that is commonly reported to be active in attention and social tasks (Decety and Lamm 2007; Corbetta et al. 2008). In the absence of detailed cytoarchitectonic measurements, it is necessary to use macroscopic boundaries that can be reliably identified as the boundaries of the ROI. A liberal ROI was drawn that incorporated all areas that have been labeled as TPJ in the literature. The dorsal boundary consisted of the lateral bank of the intraparietal sulcus. The ventral boundary consisted of the dorsal bank of the horizontal and main branches of the STS. The anterior and posterior borders were formed by the  $y = -32$  and  $y = -64$  planes of MNI space, respectively. The ROI was transformed into each participant's individual space using the FSL tool FLIRT (Jenkinson et al. 2002), using 12 degrees of freedom.

#### Data Analysis

DW-MRI data were preprocessed using tools from FDT, part of FSL (Smith et al. 2004). Eddy-current distortions were corrected using affine registration of all volumes to a target volume with no diffusion weighting. Voxel-wise estimates of the fiber orientation distribution were calculated using Bedpostx (Behrens et al. 2007). For each participant, probabilistic tractography was run from voxels within a TPJ mask to assess connectivity with every brain voxel (downsampled to 5 isotropic voxels), using a model accounting for multiple fiber orientations in each voxel (Behrens et al. 2007). The tractography approach draws a sample from each fiber orientation distribution at the current voxel and chooses the sample closest to the orientation of its previous step.

For each participant, a connectivity matrix between TPJ voxels and each voxel of the 5-mm isotropic brain voxel was derived from the data of the probabilistic tractography (Johansen-Berg et al. 2004). This matrix consists of rows indicating each TPJ voxel and columns representing each brain voxel. From this matrix, a symmetric cross-correlation matrix was generated. The size of this cross-correlation matrix is number of seeds  $\times$  number of seeds and the  $(i,j)$ th element value is the correlation between the connectivity profile of TPJ voxel  $i$

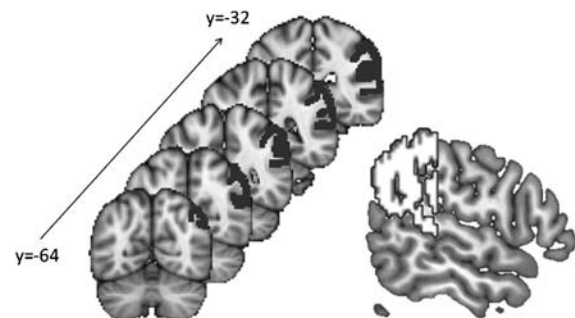


**Figure 1.** TPJ mask used in the tractography-based parcellation drawn on the structural MNI brain.

and the connectivity profile of TPJ voxel  $j$ . The rows of this cross-correlation matrix were then permuted using  $k$ -means segmentation for automated clustering to define different clusters. The goal of clustering the cross-correlation matrix is to group together regions that share the same connectivity with the rest of the brain. When performing the clustering on the cross-correlation matrix, it is potentially possible for 2 separate subregions to be clustered together based solely on their connectivity with one another rather than based on their similar connectivity to the rest of the brain. In order to increase the chances of obtaining continuous clusters, we included a weak distance constraint of 0.2 (Tomassini et al. 2007). The resulting clusters are then constrained to consist of voxels that are spatially contiguous, although the border between clusters is still guided by remote connectivity information.

The number of clusters in the  $k$ -means clustering must be set by the experimenter. Because previous investigations of TPJ provide few clues on the number of clusters we should expect, we used an iterative procedure (Beckmann et al. 2009; Mars et al. 2011) in which the number of clusters that are searched for with the  $k$ -means clustering algorithm is gradually increased as long as it is possible to identify the same component clusters in each subject. In the present study, the clustering was performed 3 times, asking for 2, 3, and 4 clusters in separate analyses.

In order to determine the structural connectivity that is driving the accepted parcellation, we performed probabilistic fiber tracking from each cluster for each participant (Behrens et al. 2007), using the following settings: 5000 samples per voxel, maximum 2000 steps, curvature threshold of 0.2, 0.5 mm step length. Following tractography from each cluster for each participant, the resulting tract images were thresholded to remove voxels with less than 250 samples passing through them and binarized. The individual tract images for each cluster of all participants were then overlaid.

### **Analysis 2: TPJ Resting State fMRI Functional Connectivity with the Rest of the Brain**

Following Analysis 1, which focused on anatomical connectivity, we turn to resting-state functional connectivity. It is important to point out that the term “functional” is here used in order to contrast it with “structural” (i.e., anatomical) connectivity. We do not mean to imply that the data used here are the result of the brain performing any particular task (or function) as would be the case in a standard functional imaging experiment. Rather, we use resting-state functional connectivity as a tool to study the connectivity of the brain. It has been shown that resting-state functional connectivity for a large part reflects anatomical connectivity (Greicius et al. 2009; Mars et al. 2011), and it has recently been employed as a tool to study connectivity of the cerebellum (O’Reilly et al. 2010), insular cortex (Deen et al. 2011), parahippocampal cortex (Vincent et al. 2010), and parietal cortex (Vincent et al. 2006; Mars et al. 2011).

### **Data Acquisition**

Human resting-state functional magnetic resonance imaging (fMRI) data and  $T_1$ -weighted images were collected for 12 healthy volunteers (9 females, age range 31–61, mean age  $\pm$  SD 43.08  $\pm$  9.17). This group of participants did not overlap with the group of participants in the diffusion-weighted imaging experiment. All participants gave informed written consent in accordance with ethical approval from the local ethics committee. Participants lay supine in a 1.5-T Siemens Sonata MR scanner. They were instructed to close their eyes and lie still. Cushions were used to reduce head motion. Whole-brain blood oxygen level-dependent fMRI data was collected for 11 min from each participant, using the following parameters: 45 axial slices, in-plane resolution  $3 \times 3$  mm, slice thickness 3 mm, no slice gap, TR = 3400 ms, TE = 41 ms, 200 volumes. A structural scan was acquired for each participant in the same session, using a  $T_1$ -weighted 3D FLASH sequence (voxel size of  $1 \times 1 \times 1$  mm).

### **Data Analysis**

Data were analyzed using tools from FSL (Smith et al. 2004). The first 6 volumes of each functional data set were discarded, after which the preprocessing was performed: motion correction, nonbrain removal, spatial smoothing (using Gaussian 5-mm full-width at half-maximum

kernel), grand-mean intensity normalization of the entire 4D data set by a single multiplicative factor, high-pass temporal filtering (Gaussian-weighted least-squares straight line fitting, with  $\sigma = 50.0$  s). For group analyses, the functional data were normalized to MNI space. This was done in 2 steps: First, each participant’s functional MRI data were registered to that participant’s structural MRI data using the linear registration tool FLIRT (normal search, 6 degrees of freedom). Second, both functional data registered to structural space, and the structural data were registered to the MNI152\_T1\_2mm\_brain MNI template brain in FSL using the linear registration tool FLIRT (normal search, 12 degrees of freedom). These settings are the default options in FSL.

To establish the functional connectivity of the TPJ subregions yielded by the tractography-based parcellation, we created three ROIs consisting of the areas of TPJ that showed overlap in 5 or more participants. A regression analyses was then run on the resting state data from each participant, following analyses procedures described previously (O’Reilly et al. 2010; Mars et al. 2011). The model consisted of 11 regressors. The first three regressors consisted of the first Eigen time series of each of the TPJ subregions reported in Analysis 1 (i.e., IPL, TPJa, and TPJp). The first Eigen time series is a single time series which best reflects coherent activity across the mask in that represents the largest amount of variance across the set of voxels in the mask. This has the advantage that if the transformation of the mask from standard space to individual space is not perfect, the activity pattern of any potentially misaligned voxels will have less of a contribution than when simply taking the average time course of activity across the mask. As such, the first Eigen time series helps prevent the mixing of signal and noise. We also calculated the major Eigen time series in masks representing the white-matter and cerebrospinal fluid (CSF; across the whole brain volume), which were derived using the FSL tissue segmentation tool FAST (Zhang et al. 2001). Time series representing head motion were extracted using MCFLIRT (Jenkinson and Smith 2001). These 8 “confounding” time series (white matter and CSF Eigen time series plus 6 time series representing head motion) were included in the first-level analyses as regressors of no interest. Individual statistical maps were then converted into MNI space for group analyses. The standard-space individual contrast maps were entered into a general linear model (GLM) analysis using a mixed-effects approach with automatic outlier downweighting (Woolrich et al. 2004; Woolrich 2008). The resulting  $Z$ -statistical images were thresholded using clusters determined by  $Z > 2.3$  and a (corrected) cluster significance threshold of  $P < 0.05$ .

### **Analysis 3: Functional Connectivity with Specific Target Areas**

We aimed to link the resulting TPJ clusters with the different patterns of functional connectivity that have been reported for TPJ in studies of social cognition and attentional switching. We specified 2 target areas, which have been shown to selectively interact with TPJ during attentional and social tasks and drew 6 mm isotropic masks at their center coordinates. First, as discussed above, the TPJ has been suggested to be part of a ventral attentional network consisting of TPJ and vPFC (Fox et al. 2006; Corbetta et al. 2008). Therefore, we defined a vPFC/Al ROI centered at (38, 18, 0). Second, we chose an amPFC ROI centered at (0, 48, 8) based on the functional connectivity study by Burnett and Blakemore (2009), which they showed interacts with TPJ during a social emotional task in which participant read and rated emotional sentences about another person. Following transformation of the masks from standard space to each participant’s functional space, we extracted the first Eigen time courses of the vPFC/Al and amPFC ROIs. These analyses were performed on the same data as Analysis 2. In addition, we acquired diffusion-weighted imaging data and resting-state functional connectivity data in 3 additional participants in order to visualize the overlap of the parcellation and functional connectivity results.

## **Results**

### **Analysis 1: Diffusion-Weighted Imaging Tractography-Based Parcellation**

The first analysis was aimed at separating the TPJ into distinct components, defined by their unique structural connections to

the rest of the brain. The connectivity profile of each voxel in the TPJ ROI was determined, and the cross-correlation matrix was calculated separately for each participant. *K*-means clustering was then used to cluster all voxels in order to group together voxels that share the same connectivity with the rest of the brain. Since the correct number of clusters is unknown, we used an iterative procedure in which we kept searching for more clusters until the consistency in location of clusters across participants broke down (Beckmann et al. 2009; Mars et al. 2011).

The results of the parcellations for the group and for each individual participant are shown in Figure 2. Grouping the voxels into 2 clusters resulted in a dorsal cluster (red in Fig. 2*a*), spanning the ventral bank of the IPL and the majority of the convexity of the IPL, and ventral cluster (blue), extending from the bank of the STS dorsally. This pattern was highly consistent across participants. Grouping the voxels into 3 clusters (Fig. 2*b*) resulted in a dorsal cluster (red) spanning the ventral bank of the IPS and a large part of the convexity of the IPL, which we will term "IPL" (center of gravity [49, -46, 46]). The region corresponds to areas, particularly the IPL area PFM, which we have previously described in detail (Mars et al. 2011). The ventral part of the ROI was partitioned into an anterior (blue, center of gravity [59, -37, 30]) and posterior (green, center of gravity [54, -55, 26]) cluster in all participants. We will refer to these clusters as the anterior and posterior TPJ (TPJa and TPJp, respectively). As can be seen in Figure 2*b*, this effect was again quite consistent across participants. When grouping the voxels into 4 clusters, the consistency across participants broke down. As can be seen in Figure 2*c*, in some participants (e.g., 2 and 4), the dorsal IPL cluster of the three-way parcellation was split up into 2 separate clusters, while for some participants (e.g., 6 and 8), the TPJa cluster of the three-way parcellation was further subdivided. Therefore, we

accepted the three-way parcellation of TPJ as a guide for further analyses.

In order to formalize the constancy of the three-way clustering between participants, we reran the clustering using the fuzzy *k*-means algorithm (Bezdek 1981). This algorithm, rather than just assigning each voxel in the TPJ seed mask to 1 of the 3 clusters, also gives a probability of each voxel belonging to each of the 3 clusters. The resulting probability maps can then be entered into a group-level regression analysis in order to get an estimate of the likelihood of each voxel belonging to each cluster. The resulting maps are standardized beta maps (Fig. 3*a*). This analysis showed that the 3 clusters are consistently present at the group level.

It is important to emphasize that the goal of the clustering analyses was not to determine exactly how many subregions TPJ consists of. Such claims are fraught because they depend on what definition of brain area is used. Rather, the goal of the present study is more hypothesis driven, namely to test the hypothesis that there is a reliable separation between loci within TPJ that preferentially participate in specific functional networks that have been previously identified. Therefore, we parcellated the TPJ into 3 clusters that could be reliably identified across a group of participants, then we examined the functional networks associated with each cluster (Analysis 2, below). Finally, we carried out additional checks to ensure that the separate TPJ clusters and networks we identified were real and not artifactual (Analysis 3, below).

In order to determine which aspects of structural connectivity are driving the three-cluster parcellation, we performed probabilistic fiber tracking from each cluster for each individual participant. The resulting tracts were then thresholded, binarized, and overlaid in standard space. As can be seen in Figure 3*b*, the 3 clusters are connected to partially different tracts. Tracts originating from the IPL cluster are most likely

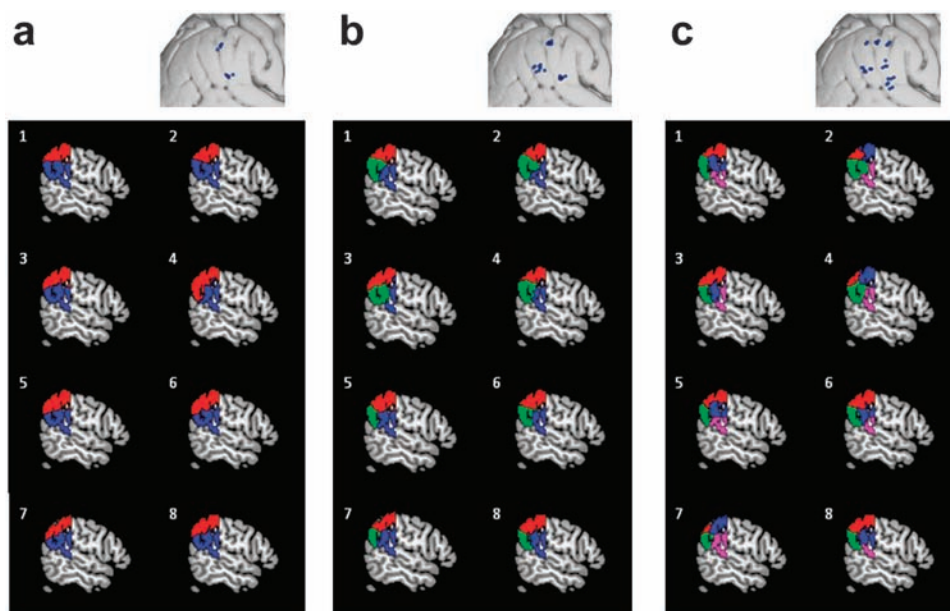


**Figure 2.** Tractography-based parcellation of the TPJ results. Results of parcellation in (a) 2, (b) 3, and (c) 4 clusters superimposed on the structural MNI brain. Top row indicates center of gravity for each cluster for each participant. Colored clusters show parcellation for each participant superimposed on the structural MNI brain. For the two-cluster parcellation, a clear separation of dorsal and ventral partitions was visible. The three-cluster parcellation showed a separation into a dorsal IPL region and 2 ventral TPJ regions. In the four-cluster parcellation, the consistency between participants began to break down.

the end up in the prefrontal cortex, whereas tracts originating in TPJa are most likely to end in the vicinity of VPFC/AI. In the temporal cortex, TPJa projections are quite widespread, including dorsal tracts possibly following the middle longitudinal fascicle, whereas tracts originating from TPJp are present in more ventral parts of the temporal cortex. However, the probabilistic nature of this fiber-tracking procedure, together with the presence of a number of crossing fiber pathways between the TPJ area and the frontal cortex and the sensitivity of fiber tracking to the distance traveled along a fiber from make it an unsuitable tool to investigate the larger cortical networks each TPJ cluster participates in. Therefore, we next turned to resting-state fMRI to study this issue.

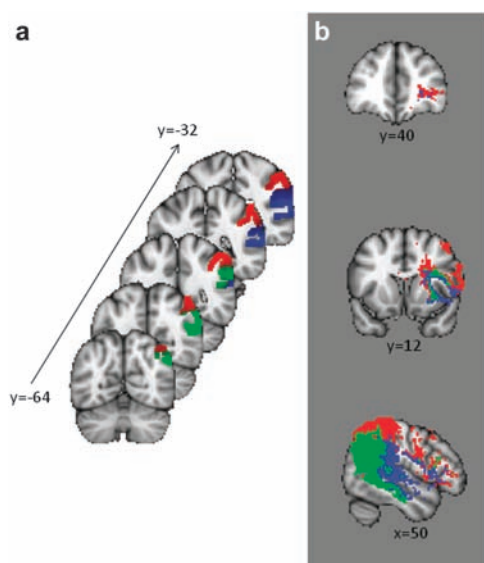


**Figure 3.** Further tractography results. (a) Second-level beta-maps illustrating the likelihood that each TPJ ROI voxel is assigned to either of the 3 TPJ subregions at the group level. Intensities scaled to standardized beta coefficients 0.35–0.75. (b) Tractography results showing tracts originating from the IPL (red), TPJa (blue), and TPJp (green) clusters. Although the probabilistic tractography algorithm shows partly overlapping tracts, clear differences are apparent in the prefrontal cortex and the temporal cortex.

### Analysis 2: TPJ Resting State fMRI Functional Connectivity with the Rest of the Brain

The second analysis was aimed at determining the larger cortical network of which each of the 3 TPJ clusters are part by means of resting-state functional connectivity. Resting-state seed masks were created for each of the 3 TPJ partitions as follows. The clusters of each participant were added together in standard space, thresholded so that only voxels belonging to any given cluster in at least 5 participants remained and binarized. The resulting seed masks were then transformed into the functional space of each of the resting-state fMRI data sets, and the time courses of the masks were extracted. Whole-brain resting-state functional connectivity with each of the 3 TPJ clusters was then assessed.

The most dorsal TPJ cluster, IPL, showed functional connectivity with bilateral IPS, middle frontal gyrus extending into the lateral anterior prefrontal cortex (aPFC), right inferior temporal gyrus, paracingulate gyrus, the anterior part of the posterior cingulate gyrus, and the right caudate nucleus (Fig. 4, Table 1). The functional connectivity between the IPL region and the lateral aPFC is similar to that noted in our previous study on functional interactions between the parietal cortex and the frontal lobes. In this previous study, functional connectivity between a middle IPL region, including the Pfm division of IPL and the lateral aPFC was especially prominent (Mars et al. 2011). However, such a pattern of functional connectivity is not reminiscent of any of interactions reported for TPJ during social cognition or attentional switching. Therefore, and because the dorsal cluster appears to correspond to the Pfm area that we have already characterized (Mars et al. 2011), we will concentrate the remainder of our analyses and discussions on the interactions of the TPJa and TPJp subdivisions.

TPJa showed functional connectivity with bilateral IPL concentrated around the supramarginal gyrus, postcentral gyrus, frontal operculum and vPFC/AI, middle frontal gyrus/frontal pole, and left cerebellum. TPJp showed functional connectivity with the amPFC/paracingulate gyrus, precuneus and posterior part of the posterior cingulate gyrus, bilateral middle temporal gyrus, temporal pole, angular gyrus/lateral occipital gyrus, and middle frontal gyrus, and left cerebellum. Thus, the 2 ventral clusters, here labeled TPJp and TPJa, show a distinct pattern of functional connectivity (Fig. 4, Table 1),

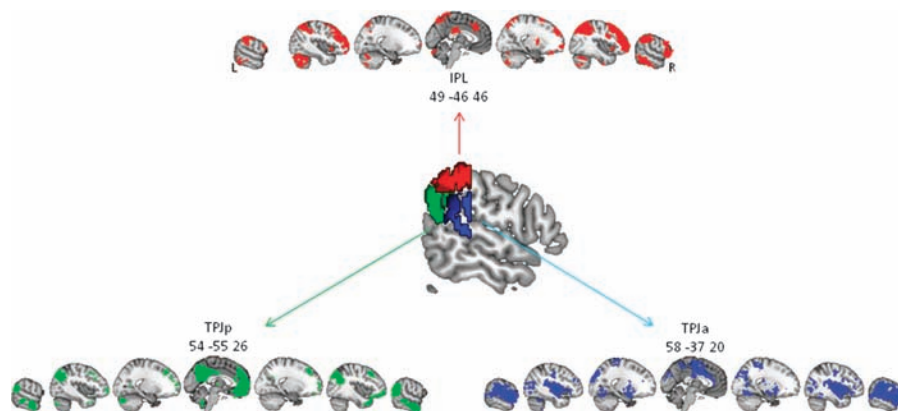


**Figure 4.** Resting-state functional connectivity of the 3 TPJ subregions. Three clusters (thresholded at voxels that belong to any given cluster in  $\geq 5$  participants) displayed on the MNI brain and their corresponding resting-state functional connectivity maps (thresholded at  $Z \geq 2.3$  and a cluster threshold of  $P < 0.05$  corrected). Coordinates indicate center of gravity of the clusters in MNI space. Unique functional connectivity patterns included those found between the dorsal TPJ region which corresponded closely to the IPL Pfm region and lateral aPFC (IPL), between TPJa and vPFC/AI, and between TPJp and amPFC and other parts of the default mode network.

with TPJp showing connectivity with areas identified with social cognition and TPJa showing patterns identified with attentional selection. The pattern of functional connectivity of TPJa, including vPFC/AI, resembles the ventral attentional network described by Corbetta and colleagues (Corbetta and Shulman 2002; Fox et al. 2006), including vPFC and AI. TPJp's pattern of functional connectivity includes a number of areas prominently activated in studies of social cognition, including the amPFC and the middle temporal gyri and temporal poles. Furthermore, the network or areas correlating with TPJp is very similar to the so-called "default mode network" often found in studies of spontaneous brain activity during rest, which includes posterior cingulate, IPL/TPJ, and amPFC (Greicius et al. 2003; Buckner et al. 2008).

**Table 1**  
Clusters showing maximal functional connectivity with each of the TPJ subregions

Anatomical region	MNI coordinates			Z statistics
	x	y	z	
IPL				
R intraparietal sulcus	42	-56	50	5.60
R middle frontal gyrus	44	20	46	5.05
L intraparietal sulcus	-36	-56	50	4.49
R inferior temporal gyrus	66	-46	-12	4.44
L middle frontal gyrus	-48	38	16	4.22
Paracingulate gyrus	4	26	46	4.11
Cingulate gyrus, posterior	-2	-18	26	3.64
Caudate/putamen	12	2	10	3.50
TPJa				
R IPL	62	-40	22	5.82
L IPL	-58	-40	24	4.54
L frontal operculum/AI	-42	2	2	4.27
Medial frontal cortex	-2	-12	52	4.22
R frontal operculum/AI	44	2	2	4.01
L middle frontal gyrus	-38	38	26	3.59
R middle frontal gyrus	34	46	26	3.58
L postcentral gyrus	-20	-38	72	3.42
L cerebellum	-30	-48	-50	3.30
TPJp				
R angular gyrus/occipital cortex	48	-60	30	6.28
Precuneus/cingulate gyrus, posterior	2	-62	38	5.27
Paracingulate gyrus	2	52	10	4.99
L angular gyrus/occipital cortex	-42	-70	38	4.98
R middle temporal gyrus	66	-44	-6	4.20
L middle temporal gyrus	-60	-44	-10	3.94
R middle frontal gyrus	42	20	44	3.82
L thalamus	-6	-16	4	3.66
L cerebellum	-4	-58	-44	3.56
R cerebellum	-22	-84	-28	3.54

### Analysis 3: Functional Connectivity with Specific Target Areas

As described above, TPJ has been implicated in different functional brain networks, one involving vPFC and AI and one involving the amPFC. One method to establish whether TPJ indeed consists of different parts based on their functional connectivity is to formally test whether functional connectivity with vPFC/AI and amPFC differentiates between the TPJa and TPJp subregions. We investigated the functional connectivity vPFC/AI and amPFC ROIs based on previously published coordinates (Fox et al. 2006; Burnett and Blakemore 2009). The difference in connectivity between TPJa and vPFC/AI on the one hand and TPJp and amPFC on the other hand was formally tested by calculating the correlation coefficients between different pairs of the first Eigen time series of these clusters for each participant. AmPFC correlated more with TPJp than with TPJa in 11 of 12 participants tested (Fig. 5a). Conversely, vPFC/AI correlated more with TPJa than with TPJp in 11 of 12 participants tested (Fig. 5b). These results were reflected in the results of statistical tests on the correlation coefficients. Paired two-sided *t*-tests on the correlation coefficients showed a stronger correlation between amPFC and TPJp than between amPFC and TPJa (0.42 vs. 0.30,  $t_{11} = 3.928$ ,  $P = 0.002$ ) and a stronger correlation between vPFC/AI and TPJa than between vPFC/AI and TPJp (0.36 vs. 0.20,  $t_{11} = 4.118$ ,  $P = 0.002$ ) (Fig. 5c). These results confirm the conclusions drawn above regarding the participation of TPJa and TPJp in different functional networks.

One important potential concern with the current study is that when one uses *k*-means to cluster the DTI data into a certain number of clusters, the algorithm will return that number of clusters, regardless of whether they are present in the data. Although the consistency of the location of these clusters across participants is reassuring (Fig. 2 and Analysis 1, above), we performed 3 additional analyses to establish whether the obtained clusters are a true reflection of differential connectivity between vPFC/AI and amPFC in the TPJ. In the first of these analyses, we investigated, for each participant, first the correlation between the vPFC/AI and then second the amPFC ROI time series with the time series of each voxel in the area spanning TPJa and TPJp, while accounting for 8 confound time series (white matter and CSF Eigen time series and 6 time series representing head movements). We then

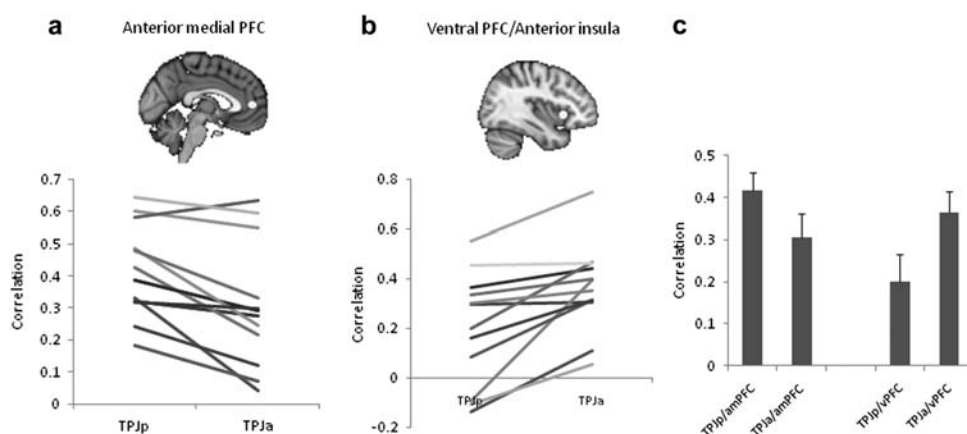


**Figure 5.** TPJa and TPJp functional connectivity with amPFC and vPFC/AI ROIs. (a, b) Correlations of TPJa and TPJp with amPFC and vPFC/AI for each participant. Locations of target ROIs are indicated by white spheres. (c) Group mean ( $\pm$ standard error of the mean) correlations.

identified, for each participant, the voxel whose time series most strongly correlated with vPFC/AI and with amPFC. As can be seen in Figure 6a, maximum correlations in TPJ with amPFC were generally more located more caudal (average MNI coordinates [50, -58, 31]) than maximum correlations with vPFC/AI (average MNI coordinates [54, -42, 25]). This is confirmed by a paired-samples *t*-test on the *y*-coordinates ( $t_{11} = 4.697, P = 0.001$ ).

Second, to further confirm that there is a separation between the functional interactions with vPFC/AI and amPFC within TPJ, we performed a GLM analysis in which we looked at functional interactions of vPFC/AI and amPFC across the whole brain, again while accounting for white matter and CSF time series. As can be seen in Figure 6b, functional interactions between vPFC/AI and amPFC were largely separated within the TPJ area, with the border between the 2 areas consistent with the border of the TPJa and TPJp clusters in the DTI parcellation analysis. Thus, the differential connectivity of these 2 cortical areas with the anterior and posterior part of the TPJ can be seen even without a formal parcellation of TPJ. There results confirm that the identification of 2 TPJ clusters is not simply an artifact of the DTI clustering algorithm, but that there is indeed a separation in the TPJ area into clusters that preferentially interact with different cortical areas.

Third, we collected both DI and resting-state fMRI data in a small group of participants, in order to confirm that the clusters resulting from the tractography-based parcellation of TPJ indeed differentially interact with vPFC/AI and amPFC in the same participants. We collected a structural scan, resting-state functional MRI, and diffusion-weighted imaging data (in one single session on a 3-T Siemens Trio using the same parameters as in the previous data sets) in 3 participants (all right-handed; 2 female; age range 25–31 years), who were not part of either of the data sets used in the previous analyses. We performed the same preprocessing, fiber tracking, and 3 cluster *k*-means clustering as in Analysis 1 on their diffusion-weighted imaging data and the same resting-state functional connectivity analysis looking at whole-brain interactions of amPFC and vPFC/AI as described above. As can be seen in Figure 7, for all 3 participants, the TPJp cluster overlapped with the voxels whose correlated with the amPFC time course. Voxels whose activity correlated with vPFC/AI are found in both the IPL and TPJa cluster but importantly not in TPJp. These results are similar for all participants, although the third participant shows significant functional connectivity with amPFC in areas ventral to the ventral border of the TPJ mask, suggesting that perhaps for this participant the ROI should have extended more ventrally.

## Discussion

The present study was aimed at exploring the possibility that the cortical expanse termed TPJ consists of subdivisions that can be identified on the basis of structural and functional connectivity. We defined TPJ on the basis of an anatomical mask including all areas labeled as TPJ in previous studies (Mort et al. 2003; Decety and Lamm 2007; Corbetta et al. 2008). This TPJ ROI covered the cortex from the ventral bank of the IPS to the dorsal bank of the horizontal and main branches of the STS. We submitted this TPJ ROI to an observer-independent, data-driven tractography-based parcellation. The most consistent parcellation revealed 3 subdivisions. There were a large dorsal cluster spanning the ventral bank of the IPS and the convexity of the IPL and 2 ventral clusters, TPJa and TPJp. Next, we assessed the resting-state functional connectivity of each of these clusters with the rest of the brain. The activity of the IPL cluster correlated strongly with a network including the lateral anterior PFC. The TPJa cluster was coupled to the vPFC and AI, areas previously associated with the ventral attentional network (Corbetta and Shulman 2002). The TPJp cluster was coupled to the amPFC and the posterior cingulate and precuneus, areas previously associated with both social cognition, specifically mentalizing, and the default mode network (Gusnard and Raichle 2002; Buckner et al. 2008). These results indicate that TPJ is not a homogenous region but that it can be subdivided into at least 2 subregions, which can also be distinguished from the adjacent IPL, on the basis of its estimated structural and functional connectivity.

Both tractography-based parcellation and resting-state functional connectivity profiles suggest a functional dichotomy of the TPJ consistent with the 2 broad functions previously associated with this region, namely attentional selection and mental state predictions (Saxe 2006; Corbetta et al. 2008). As discussed in the Introduction, the debate on a potential dissociation between these 2 functions in the TPJ has been particularly prominent. However, this is not to say that the TPJ has not been implicated in other, perhaps related, cognitive functions. For instance, TPJ has recently been reported to be involved in processing uncertainty and empathy (Singer et al. 2009; Lamm and Singer 2010) and in maintaining a coherent sense of one's body as compared with noncorporeal objects (Decety and Grèzes 2006; Tsakiris et al. 2008; Blanke and Metzinger 2009). The current study may provide an anatomical basis for future localization and interpretation of results obtained in paradigms probing these cognitive functions.

It should be emphasized that the present results cannot resolve whether the functional anatomical dichotomy between

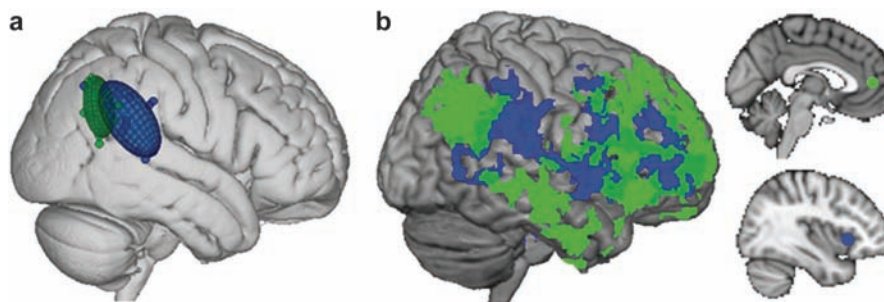


**Figure 6.** Whole-brain functional connectivity of amPFC and vPFC/AI ROIs. (a) Locations of maximal correlation with vPFC/AI (green dots) and amPFC (blue dots) within the combined TPJa and TPJp area. Ellipsoids represent 95% confidence interval. (b) Whole-brain GLM results, showing voxels whose time course correlates with vPFC/AI (green) and amPFC (blue), thresholded at  $Z \geq 2.3$  and a (corrected) cluster significance of  $P \leq 0.05$ .

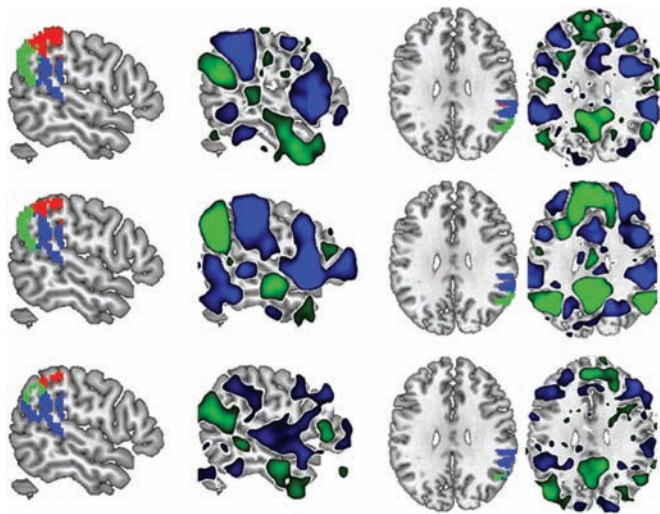


**Figure 7.** Diffusion-weighted imaging tractography-based parcellation (cf. Fig. 2) and whole-brain functional connectivity of amPFC and vPFC/AI ROIs (cf. Fig. 6) for 3 individual participants. Three cluster parcellation shown on sagittal and axial slices (left columns) showing the division into IPL, TPJa, and TPJp clusters. Functional connectivity results shown on the same slices (right columns) illustrate that the voxels whose activity correlates with amPFC (green) mostly overlap with TPJp, while voxels whose activity correlates with vPFC/AI (blue) mostly overlap with TPJp and IPL. Functional connectivity maps thresholded at the liberal threshold of  $Z \geq 1$  for each participant.

TPJa and TPJp reflects a computational divide. For instance, TPJa and TPJp may perform similar computational functions but on different types of information. Consistent with this notion that analogous processes might be apparent in different parts of the cortex, a social prediction error was shown to activate a region within the current TPJp cluster (Behrens et al. 2008) and similar signals, albeit relating to visual events, have been suggested to underlie attentional processes (Mars et al. 2008; Rushworth, Mars, Summerfield, 2009), possibly in TPJa. Accordingly, the present results are not inconsistent with the view that attentional selection and social cognition share computational properties in the TPJ (Corbetta et al. 2008; Mitchell 2008).

The TPJ ROI used in the present study was intended to be inclusive and to incorporate the territory commonly referred to by the TPJ designation. It therefore partly overlapped with the lateral parietal cortex region that we have previously characterized (Mars et al. 2011), and it is informative to discuss the relationship between the 2 studies here. Both TPJa and TPJp were ventral to the boundary of the IPL ROI used in the previous study. The dorsal IPL cluster of the present study overlapped with part of the IPL region investigated in the previous study. Mars et al. (2011) showed that the IPL could be divided into at least 5 clusters using the same methods of diffusion-weighted imaging and resting-state functional connectivity as in the present study. Indeed, the same data sets were used in both studies. The IPL regions corresponded closely to those previously reported in a cytoarchitectonic study (Caspers et al. 2006, 2008). The IPL cluster reported in the present study overlapped with the third most posterior IPL cluster in the previous study, PFm, spanning the posterior supramarginal gyrus. As in the current study, Mars et al. (2011) reported that PFm exhibited strong functional connectivity with aPFC.

There is one major interpretational limitation of the analyses presented in the present paper that requires discussion. It is imperative to note that the clustering approach used here does not resolve the problem of exactly how many subregions TPJ consists of. We have shown that there is a consistent result when parcellating our ROI into 3 clusters, but it is possible—indeed, it is likely—that a more fine-grained parcellation is possible. As discussed above, we and other have already shown that IPL can be subdivided into subregions based on connectivity (Mars et al. 2011) and cytoarchitecture (Caspers et al. 2008). The claim of the current study is thus not that TPJ consists of exactly 3 subregions but is more nuanced. We claim that the cortical expanse TPJ is not a uniform brain area but that different parts of this region preferentially interact with different parts of the cortex, specifically with vPFC/AI and amPFC. We hope these results can help interpret future imaging studies on TPJ and constrain their interpretation.

Two anatomical issues remain unaddressed in the present study. First, there is to our knowledge no study formally comparing TPJ in humans and non-human primates. Processing of information relevant to social behavior, such as faces (Perrett et al. 1992), auditory cues (Romanski and Averbeck 2009), and even gaze direction and body posture (Lorincz et al. 2005), has been reported along the STS in macaques. Such processes might be related to those that occur in the TPJ in humans. In this context, it is noteworthy that the IPL and parts of the temporal cortex have expanded disproportionately in the human, as compared with the monkey, cortex (Van Essen and Dierker 2007; Rushworth, Boorman, Mars, 2009), which might have resulted in a displacement of some of the homologues of the brain areas identified in the monkey. Thus, direct comparison of the human TPJ and areas in the macaque brain remains an open issue. The second remaining issue concerns lateralization. The current study focuses solely on the right TPJ because that hemisphere has been the one most frequently implicated in the ventral attention network (Corbetta and Shulman 2002) and in social cognition (Decety and Lamm 2007). As with the more general organization of TPJ, it is unclear how this lateralization developed during evolution, although lateralization seems to be particularly pronounced in the human brain (Passingham 2008).

In summary, in this study, we set out to test the hypothesis that TPJ can be divided into distinct subregions based on their structural and functional connectivity. We have shown that there is evidence for at least 3 subregions. A dorsal area that overlaps with the middle part of the IPL, and 2 ventral areas which can be distinguished on the basis of their participating in different cortical networks involving vPFC/AI and amPFC. These results can be used to constrain future hypotheses on TPJ structure and function and may prove helpful in between-species comparisons.

## Notes

*Conflict of Interest*: None declared.

## Funding

Medical Research Council UK (G0802146) (to R.B.M. and M.F.S.R.); VICI grant from the Nederlandse Organisatie voor Wetenschappelijk Onderzoek (NWO, 453-08-002) (to I.T.).

## References

- Anwander A, Tittgemeyer M, von Cramon DY, Friederici AD, Knosche TR. 2007. Connectivity-based parcellation of Broca's area. *Cereb Cortex*. 17:816–825.
- Astafiev SV, Shulman GL, Corbetta M. 2006. Visuospatial reorienting signals in the human temporo-parietal junction are independent of response selection. *Eur J Neurosci*. 23:591–596.
- Beckmann M, Johansen-Berg H, Rushworth MF. 2009. Connectivity-based parcellation of human cingulate cortex and its relation to functional specialization. *J Neurosci*. 29:1175–1190.
- Behrens TE, Hunt LT, Woolrich MW, Rushworth MF. 2008. Associative learning of social value. *Nature*. 456:245–249.
- Behrens TE, Johansen-Berg H, Jbabdi S, Rushworth MF, Woolrich MW. 2007. Probabilistic diffusion tractography with multiple fibre orientations: what can we gain? *Neuroimage*. 34:144–155.
- Bezdek JC. 1981. Pattern recognition with fuzzy objective function algorithms. New York: Plenum Press.
- Blanke O, Metzinger T. 2009. Full-body illusions and minimal phenomenal selfhood. *Trends Cogn Sci*. 13:7–13.
- Buckner RL, Andrews-Hanna JR, Schacter DL. 2008. The brain's default network. Anatomy, function, and relevance to disease. *Ann N Y Acad Sci*. 1124:1–38.
- Burnett S, Blakemore SJ. 2009. Functional connectivity during a social emotion task in adolescents and in adults. *Eur J Neurosci*. 29:1294–1301.
- Caspers S, Eickhoff SB, Geyer S, Scheperjans F, Mohlberg H, Zilles K, Amunts K. 2008. The human inferior parietal lobule in stereotaxic space. *Brain Struct Funct*. 212:481–495.
- Caspers S, Geyer S, Schleicher A, Mohlberg H, Amunts K, Zilles K. 2006. The human inferior parietal cortex: cytoarchitectonic parcellation and interindividual variability. *Neuroimage*. 33:430–448.
- Corbetta M, Patel G, Shulman GL. 2008. The reorienting system of the human brain: from environment to theory of mind. *Neuron*. 58:306–324.
- Corbetta M, Shulman GL. 2002. Control of goal-directed and stimulus-driven attention in the brain. *Nat Rev Neurosci*. 3:201–215.
- Decety J, Grèzes J. 2006. The power of simulation: imagining one's own and other's behavior. *Brain Res*. 1079:4–14.
- Decety J, Lamm C. 2007. The role of the right temporoparietal junction in social interaction: how low-level computational processes contribute to meta-cognition. *Neuroscientist*. 13:580–593.
- Deen B, Pitskel NB, Pelphrey KA. 2011. Three systems of insular functional connectivity identified with cluster analysis. *Cereb Cortex*. 21:1498–1506.
- Den Ouden HEM, Frith U, Frith C, Blakemore SJ. 2005. Thinking about intentions. *Neuroimage*. 28:787–796.
- Fletcher PC, Happe F, Frith U, Baker SC, Dolan RJ, Frackowiak RS, Frith CD. 1995. Other minds in the brain: a functional imaging study of "theory of mind" in story comprehension. *Cognition*. 57:109–128.
- Fox MD, Corbetta M, Snyder AZ, Vincent JL, Raichle ME. 2006. Spontaneous neuronal activity distinguishes human dorsal and ventral attention systems. *Proc Natl Acad Sci U S A*. 103:13560–13560.
- Frith CD, Frith U. 2006. The neural basis of mentalizing. *Neuron*. 50:531–534.
- Greicius MD, Krasnow B, Reiss AL, Menon V. 2003. Functional connectivity in the resting brain: a network analysis of the default mode hypothesis. *Proc Natl Acad Sci U S A*. 100:253–258.
- Greicius MD, Supekar K, Menon V, Dougherty RF. 2009. Resting-state functional connectivity reflects structural connectivity in the default mode network. *Cereb Cortex*. 19:72–78.
- Gusnard DA, Raichle ME. 2002. Searching for a baseline: functional imaging and the resting human brain. *Nat Rev Neurosci*. 2:685–694.
- Hampton AN, Bossaerts P, O'Doherty JP. 2008. Neural correlates of mentalizing-related computations during strategic interactions in humans. *Proc Natl Acad Sci U S A*. 105:6741–6746.
- Himmelbach M, Erb M, Karnath HO. 2006. Exploring the visual word: the neural substrate of spatial orienting. *Neuroimage*. 32:1747–1759.
- Jenkinson M, Bannister P, Brady M, Smith S. 2002. Improved optimization for the robust and accurate linear registration and motion correction of brain images. *Neuroimage*. 17:825–841.
- Jenkinson M, Smith S. 2001. A global optimisation method for robust affine registration of brain images. *Med Image Anal*. 5:143–156.
- Johansen-Berg H, Behrens TE, Robson MD, Drobniak I, Rushworth MF, Brady JM, Smith SM, Higham DJ, Matthews PM. 2004. Changes in connectivity profiles define functionally distinct regions in human medial frontal cortex. *Proc Natl Acad Sci U S A*. 101:13335–13340.
- Klein JC, Behrens TEJ, Robson MD, Mackay CE, Higham DJ, Johansen-Berg H. 2007. Connectivity-based parcellation of human cortex using diffusion MRI: establishing reproducibility, validity and observer independence in BA 44/45 and SMA/pre-SMA. *Neuroimage*. 34:204–211.
- Knight RT, Scabini D, Woods DL, Clayworth CC. 1989. Contributions of temporal-parietal junction to the human auditory P3. *Brain Res*. 502:109–116.
- Lamm C, Singer T. 2010. The role of anterior insular cortex in social emotions. *Brain Struct Funct*. 214:579–591.
- Lorincz EN, Jellema T, Gómez JC, Barraclough N, Xiao D, Perrett DI. 2005. Do monkeys understand actions and minds of others? Studies of single cells and eye movements. In: Dehaene S, Duhamel JR, Hauser MD, Rizzolatti G, editors. From monkey brain to human brain: A Fyssen Foundation symposium. Cambridge (MA): MIT Press. p. 189–210.
- Mars RB, Debener S, Gladwin TE, Harrison LM, Haggard P, Rothwell JC, Bestmann S. 2008. Trial-by-trial fluctuations in the event-related electroencephalogram reflect dynamic changes in the degree of surprise. *J Neurosci*. 28:12539–12545.
- Mars RB, Jbabdi S, Sallet J, O'Reilly JX, Crosson PL, Olivier E, Noonan MP, Bergmann C, Mitchell AS, Baxter MG, et al. 2011. Diffusion-weighted imaging tractography-based parcellation of the human parietal cortex and comparison with human and macaque resting state functional connectivity. *J Neurosci*. 31:4087–4100.
- Meister IG, Wienemann M, Buelte D, Grunewald C, Sparing R, Dambeck N, Boroojerdi B. 2006. Hemiextinction induced by transcranial magnetic stimulation over the right temporo-parietal junction. *Neuroscience*. 142:119–123.
- Mitchell JP. 2008. Activity in right temporo-parietal junction is not selective for theory-of-mind. *Cereb Cortex*. 18:262–271.
- Mort DJ, Malhotra P, Mannan SK, Rorden C, Pambakian A, Kennard C, Husain M. 2003. The anatomy of visual neglect. *Brain*. 126:1986–1997.
- Nieuwenhuis S, Aston-Jones G, Cohen JD. 2005. Decision making, the P3, and the locus coeruleus-norepinephrine system. *Psychol Bull*. 131:510–532.
- O'Reilly JX, Beckmann CF, Tomassini V, Ramnani N, Johansen-Berg H. 2010. Distinct and overlapping functional zones in the cerebellum defined by resting state functional connectivity. *Cereb Cortex*. 20:953–965.
- Passingham R. 2008. What is special about the human brain?. Oxford: Oxford University Press.
- Passingham RE, Stephan KE, Kotter R. 2002. The anatomical basis of functional localization in the cortex. *Nat Rev Neurosci*. 3:606–616.
- Perrett DI, Hietanen JK, Oram MW, Benson PJ, Rolls ET. 1992. Organization and functions of cells responsive to faces in the temporal cortex. *Philos Trans R Soc Lond B Biol Sci*. 335:23–30.
- Romanski LM, Averbeck BB. 2009. The primate cortical auditory system and neural representations of conspecific vocalizations. *Annu Rev Neurosci*. 32:315–346.
- Rushworth MFS, Boorman E, Mars RB. 2009. Comparing brain connections in different species using diffusion weighted imaging. In: Johansen-Berg H, Behrens TEJ, editors. Diffusion MRI. From quantitative measurement to in vivo neuroanatomy. Amsterdam (The Netherlands): Academic Press. p. 445–460.
- Rushworth MFS, Mars RB, Summerfield C. 2009. General mechanisms for making decisions? *Curr Opin Neurobiol*. 19:75–83.
- Saxe R. 2006. Uniquely human social cognition. *Curr Opin Neurobiol*. 16:235–239.
- Saxe R, Kanwisher N. 2003. People thinking about thinking people. The role of the temporo-parietal junction in "theory of mind". *Neuroimage*. 19:1835–1842.
- Saxe R, Wexler A. 2005. Making sense of another mind: the role of the right temporo-parietal junction. *Neuropsychologia*. 43:1391–1399.

- Scholz J, Triantafyllou C, Whitfield-Gabrieli S, Brown EN, Saxe R. 2009. Distinct regions of right temporo-parietal junction are selective for theory of mind and exogenous attention. *PLoS One*. 4:e4869.
- Singer T, Critchley HD, Preuschoff K. 2009. A common role of insula in feelings, empathy and uncertainty. *Trends Cogn Sci*. 13:334-340.
- Smith SM, Jenkinson M, Woolrich MW, Beckmann CF, Behrens TE, Johansen-Berg H, Bannister PR, De Luca M, Drobnjak I, Flitney DE, et al. 2004. Advances in functional and structural MR image analysis and implementation as FSL. *Neuroimage*. 23(Suppl 1): S208-S219.
- Tomassini V, Jbabdi S, Klein JC, Behrens TE, Pozzilli C, Matthews PM, Rushworth MF, Johansen-Berg H. 2007. Diffusion-weighted imaging tractography-based parcellation of the human lateral premotor cortex identifies dorsal and ventral subregions with anatomical and functional specializations. *J Neurosci*. 27:10259-10269.
- Tsakiris M, Constantini M, Haggard P. 2008. The role of the right temporo-parietal junction in maintaining a coherent sense of one's body. *Neuropsychologia*. 46:3014-3018.
- Van Essen DC, Dierker DL. 2007. Surface-based and probabilistic atlases of primate cerebral cortex. *Neuron*. 56:209-225.
- Vincent JL, Kahn I, Van Essen DC, Buckner RL. 2010. Functional connectivity of the macaque posterior parahippocampal cortex. *J Neurophysiol*. 103:793-800.
- Vincent JL, Snyder AZ, Fox MD, Shannon BJ, Andrews JR, Raichle ME, Buckner RL. 2006. Coherent spontaneous activity identifies a hippocampal-parietal memory network. *J Neurophysiol*. 96:3517-3531.
- Woolrich M. 2008. Robust group analysis using outlier inference. *Neuroimage*. 41:286-301.
- Woolrich MW, Behrens TE, Beckmann CF, Jenkinson M, Smith SM. 2004. Multilevel linear modelling for fMRI group analysis using Bayesian inference. *Neuroimage*. 21:1732-1747.
- Yamaguchi S, Knight RT. 1991. Anterior and posterior association cortex contributions to the somatosensory P300. *J Neurosci*. 11:2039-2054.
- Zhang Y, Brady M, Smith S. 2001. Segmentation of brain MR images through a hidden Markov random field model and the expectation maximization algorithm. *IEEE Trans Med Imaging*. 20:45-57.